


# HWENO Schemes Based on Compact Difference for Hyperbolic Conservation Laws

Zhan Ma<sup>1</sup>  · Song-Ping Wu<sup>1</sup>

Received: 21 August 2017 / Revised: 29 January 2018 / Accepted: 31 January 2018 /  
Published online: 6 February 2018  
© Springer Science+Business Media, LLC, part of Springer Nature 2018

**Abstract** In this paper, in order to simplify the high order Hermite weighted essentially non-oscillatory (HWENO) finite difference schemes of Liu and Qiu (J Sci Comput 63:548–572, 2015), a new type of HWENO schemes based on compact difference schemes, termed CHWENO (compact HWENO) schemes, is proposed for solving both one and two dimensional hyperbolic conservation laws. The idea of reconstruction in CHWENO schemes is similar to HWENO schemes, however the first derivative values of solution are solved by the compact difference method and only one numerical flux is used in CHWENO schemes, while the derivative equation is needed to be solved and two numerical fluxes are used in HWENO schemes. Compared with the original finite difference weighted essentially non-oscillatory schemes, CHWENO schemes maintain the compactness of HWENO schemes, which means that only three points are needed for a fifth order CHWENO schemes. Compared with the HWENO schemes, CHWENO schemes avoid solving the complex derivative equations, which can considerably expedite calculating speed. Several numerical tests, including the 1D shock density wave interaction problem and 2D Riemann problem, are presented to demonstrate the efficiency of CHWENO schemes.

**Keywords** HWENO scheme · Compact difference · CHWENO reconstruction · High order accuracy

**Mathematics Subject Classification** 65M06 · 65M99 · 35L65

---

The research was supported by NSFC Grant 91530325.

---

✉ Zhan Ma  
mzyao925@163.com

Song-Ping Wu  
wuspings825@163.com

<sup>1</sup> School of Aeronautics Science and Engineering, Beihang University, Beijing 100191, People's Republic of China

## 1 Introduction

In this paper, we design and test the finite difference compact Hermite weighted essentially non-oscillatory (CHWENO) schemes for solving the nonlinear hyperbolic conservation laws of the type:

$$\mathbf{u}_t + \operatorname{divf}(\mathbf{u}) = 0. \quad (1.1)$$

Because of their nonlinear characteristics, there are several difficulties in solving these equations by mathematical methods. Thus in application, such as fluid dynamics, we always solve these problems by numerical methods. On the one hand, in order to reduce the grid numbers and improve the efficiency in the calculation, numerical methods of high-order accuracy are undoubtedly the best choices. On the other hand, when meeting with the problems with strong discontinuities, the high-order numerical methods cannot maintain the good characteristics, even the oscillations may appear near the discontinuities and influence the whole solutions. Therefore developing numerical methods of high-order accuracy, high efficiency and high robustness has aroused wide interest of researchers and practitioners. At the present stage, many numerical methods of high-order accuracy have been devised to solve these problems. In this paper, what we would like to mention are essentially non-oscillatory (ENO) schemes, weighted ENO (WENO) schemes and Hermite WENO (HWENO) schemes.

In 1987, in order to overcome the drawbacks of total variation diminishing (TVD) schemes [7], finite volume ENO schemes were first proposed by Harten, Osher, Engquist and Chakravarthy [8,9]. ENO schemes choose the smoothest stencil among all the candidates to approximate the fluxes, which aims to get a high order accuracy and eliminate the spurious oscillation near the discontinuities. In 1988 and 1989, Shu and Osher devised the finite difference ENO schemes [27,28], which can simplify the reconstruction from cell averages to point values in the finite volume ENO schemes. Then Christofi [3], Iske and Sonner [10] proposed ENO schemes on the basis of non-polynomial function reconstruction.

The first finite volume WENO schemes, which were introduced by Liu and Osher [20] in 1994, are based on ENO schemes. The key idea of WENO schemes is to use a convex combination of all the candidate stencils. Each of candidate stencils is assigned a nonlinear weight which depends on local smoothness of the numerical solution on the candidate stencils and the optimal weights. In this way, WENO schemes can achieve a higher order accuracy, which means that an  $r$ th-order ENO scheme leads to a  $(2r - 1)$ th-order WENO scheme, and keep a non-oscillatory property near the discontinuities. In 1996, Shu and Jiang introduced third and fifth order finite difference WENO schemes [12] in multi space dimensions. WENO schemes retain the two major benefits of ENO schemes: uniformly high order accuracy and an essentially non-oscillatory shock transition, which make them excellent methods for solving many problems with strong shocks. In addition, WENO schemes are more efficient than ENO schemes, because WENO schemes completely remove the logical statement in the stencil choosing steps of ENO schemes. Then Jiang and Osher et al. [11,14,21] developed ENO and WENO schemes for Hamilton–Jacobi equations. Balsara and Shu [2] proposed WENO schemes with increasingly high order of accuracy.

In 2004, Qiu and Shu had constructed a class of fifth-order finite volume WENO schemes based on the Hermite polynomials, termed HWENO schemes [22], for solving the 1D nonlinear hyperbolic conservation laws and serving as the limiters of the Runge–Kutta Discontinuous Galerkin (RKDG) methods. Unlike the Lagrange interpolation in the original WENO schemes, both the function and its first derivative values are evolved in the reconstruction of HWENO schemes. Then HWENO schemes were applied to two-dimensional situation [23,30]. In 2015, Liu and Qiu had proposed fifth-order finite difference HWENO

schemes [16] and then presented an alternative approach to reconstruct the numerical fluxes [17]. HWENO schemes are more compact than WENO schemes on the same order of accuracy in smooth regions. However, the drawback of HWENO schemes is to solve an extra derivative equation in every step, which causes that the HWENO schemes require about double computing time of original WENO schemes under the same grid numbers.

In 1989, Dennis and Hundson [5] proposed a fourth-order compact difference scheme in convection-diffusion problems. This scheme could obtain more accurate results by coarser meshes. In 1992, Lele [15] firstly developed compact difference schemes with spectral-like resolution on the basis of previous work. He proposed a central sixth-order compact difference scheme with five points, which could attain the same accuracy of spectrum method. Then a compact-ENO scheme for shock-turbulence interaction problems was introduced by Adams and Shariff [1] in 1996. Next year, Gaitonde and Shang [6] proposed optimized compact-difference-based finite-volume schemes, which facilitated the development of high order accurate compact difference. Then Sengupta et al. [4, 13, 25] developed a type of upwind compact difference schemes and applied them in many areas. In 2013, Liu et al. [18] proposed a new class of linear central compact difference schemes by using function values on both grid nodes and cell centers. Then in 2015, Xuliang Liu et al. [19] developed a new class of nonlinear central compact difference schemes, where numerical fluxes at cell centers are obtained by a hybrid weighted nonlinear interpolation.

To improve the efficiency of HWENO schemes, a class of fifth-order finite difference compact HWENO (CHWENO) schemes is presented in this paper. Instead of solving the derivative equations, CHWENO schemes use the compact difference methods to obtain the derivative values in the process of reconstruction. Thus CHWENO schemes only use one numerical flux in the calculation, while HWENO schemes need to get two numerical fluxes. On the one hand, CHWENO schemes maintain the compactness of HWENO schemes. Specifically, five points are needed to get a fifth-order WENO (WENO5) numerical flux, while only three points are needed for both a fifth-order HWENO (HWENO5) and a fifth-order CHWENO (CHWENO5) numerical flux. On the other hand, CHWENO schemes can considerably increase the calculating speed because the derivative equations have been removed. In two dimensional cases, CHWENO schemes can avoid order reduction like HWENO schemes.

The organization of this paper is as follow. In Sect. 2, we will describe the reconstruction process of finite difference CHWENO schemes for one dimensional situations and the compact difference methods that are used to get the derivative values. In Sect. 3, we extend the CHWENO schemes to two-dimensional cases. In Sect. 4, we test the characteristics of CHWENO schemes by some typical numerical experiments. Concluding remarks are given in Sect. 5.

## 2 Descriptions of CHWENO Schemes in One-Dimensional Case

### 2.1 Finite Difference WENO Schemes of Jiang and Shu

In this section, we firstly introduce the finite difference WENO schemes of Jiang and Shu [12] as the basis, because WENO schemes are general frameworks for the reconstruction approaches. Consider the one-dimensional scalar conservation laws of (1.1):

$$\begin{cases} u_t + f(u)_x = 0, & x \in (-\infty, \infty), t \in (0, \infty), \\ u(x, 0) = u_0(x), & x \in (-\infty, \infty). \end{cases} \quad (2.1)$$

We discretize the space into uniform intervals of size  $\Delta x$  and then define  $x_j = j\Delta x$ . The variable quantities at  $x_j$  will be identified by the subscript  $j$ . The spacial operator of WENO schemes [12], which approximate  $-f(u)_x$ , will take the conservative form

$$\frac{du_j(t)}{dt} = -\frac{\bar{f}_{j+\frac{1}{2}} - \bar{f}_{j-\frac{1}{2}}}{\Delta x}, \tag{2.2}$$

where the numerical flux  $\bar{f}_{j+\frac{1}{2}}$  is the high order approximation of function  $F(x + 1/2)$ , which is defined implicitly by

$$f(u(x)) = \frac{1}{\Delta x} \int_{x-\frac{1}{2}\Delta x}^{x+\frac{1}{2}\Delta x} F(\xi) d\xi. \tag{2.3}$$

Then we have

$$f(u)_x|_{x=x_j} = \frac{1}{\Delta x} [F(x_{j+1/2}) - F(x_{j-1/2})]. \tag{2.4}$$

The numerical flux  $\bar{f}_{j+\frac{1}{2}}$  satisfying

$$\bar{f}_{j+\frac{1}{2}} = F(x_{j+1/2}) + O(\Delta x^r), \tag{2.5}$$

makes the scheme (2.22)  $r$ th order accuracy.

For the robustness of numerical schemes, we usually divide the numerical flux into positive and negative part [8,27]:

$$f(u) = f^+(u) + f^-(u), \tag{2.6}$$

where  $df(u)^+/du \geq 0$  and  $df(u)^-/du \leq 0$ . One example is the global Lax–Friedrichs (LF) flux splitting

$$f^+(u) = \frac{1}{2} [f(u) + \alpha u], \quad f^-(u) = \frac{1}{2} [f(u) - \alpha u], \tag{2.7}$$

where  $\alpha = \max |f'(u)|$  and the maximum is gotten over the whole range of  $u$ . Hence, we have the numerical flux  $\bar{f}_{j+\frac{1}{2}}$  been split into two parts:

$$\bar{f}_{j+\frac{1}{2}} = \bar{f}_{j+\frac{1}{2}}^+ + \bar{f}_{j+\frac{1}{2}}^-. \tag{2.8}$$

Here, because of the mirror symmetry, we will only give the reconstruction of positive flux part  $\bar{f}_{j+\frac{1}{2}}^+$  in this paper. The reconstruction of negative part will not be shown.

Like ENO schemes,  $\bar{f}_{j+\frac{1}{2}}^+$  can be also obtained in  $r$  candidate stencils in WENO schemes. Here we denote the  $r$  candidate stencils by  $S_k, k = 0, 1, \dots, r - 1$ , where

$$S_k = (I_{j+k-r+1}, I_{j+k-r+2}, \dots, I_{j+k}).$$

The difference is that ENO schemes only use the smoothest stencil, while WENO schemes use all stencils. In WENO schemes, each of candidate stencils is assigned a nonlinear weight which depends on local smoothness of the numerical solution on the candidate stencils and the optimal weights. Then we take fifth-order finite difference WENO schemes for an example to illustrate the optimal weights and smoothness measurement.

In fifth-order finite difference WENO schemes, there are three candidate stencils:  $S_1 = \{I_{j-2}, I_{j-1}, I_j\}$ ,  $S_2 = \{I_{j-1}, I_j, I_{j+1}\}$ ,  $S_3 = \{I_j, I_{j+1}, I_{j+2}\}$ , which are used to structure a bigger stencil  $S = S_1 \cup S_2 \cup S_3 = \{I_{j-2}, I_{j-1}, I_j, I_{j+1}, I_{j+2}\}$ .

For the smaller stencil  $S_i$ , we use Lagrange polynomials to formulate the function  $p_i(x)$  to get the function value at the half nodes  $x_{j+1/2}$ . Hence, we have

$$\begin{aligned} p_1(x_{j+1/2}) &= \frac{1}{3}f_{j-2} - \frac{7}{6}f_{j-1} + \frac{11}{6}f_j, \\ p_2(x_{j+1/2}) &= -\frac{1}{6}f_{j-1} + \frac{5}{6}f_j + \frac{1}{3}f_{j+1}, \\ p_3(x_{j+1/2}) &= \frac{1}{3}f_j + \frac{5}{6}f_{j+1} - \frac{1}{6}f_{j+2}. \end{aligned} \tag{2.9}$$

For the bigger stencil  $S$ , we can also get the function  $q(x)$  through Lagrange polynomials. Then we get a fifth-order numerical flux

$$q\left(x_{j+\frac{1}{2}}\right) = \frac{1}{30}f_{j-2} - \frac{13}{60}f_{j-1} + \frac{47}{60}f_j + \frac{9}{20}f_{j+1} - \frac{1}{20}f_{j+2}, \tag{2.10}$$

which could be constructed by the convex combination of the smaller stencils as follow:

$$\begin{cases} q(x_{j+1/2}) = \sum_1^3 C_i^+ p(x_{j+1/2}), \\ \sum_1^3 C_i^+ = 1. \end{cases} \tag{2.11}$$

We could get

$$C_1^+ = \frac{1}{10}, \quad C_2^+ = \frac{3}{5}, \quad C_3^+ = \frac{3}{10} \tag{2.12}$$

We also need to compute the smoothness measurement, indicated by  $IS_i^+$  for stencil  $S_i$ . This part will be described in detail later. Then we assume

$$\alpha_r^+ = \frac{C_r^+}{(\varepsilon + IS_r^+)^2} \quad (r = 1, 2, 3), \tag{2.13}$$

and get the weight function

$$\omega_r^+ = \frac{\alpha_r^+}{\alpha_1^+ + \alpha_2^+ + \alpha_3^+} \quad (r = 1, 2, 3). \tag{2.14}$$

Finally we can get the WENO reconstruction approximation

$$\tilde{f}_{j+\frac{1}{2}}^+ = \omega_1^+ p_1^+ + \omega_2^+ p_2^+ + \omega_3^+ p_3^+, \tag{2.15}$$

and the numerical flux

$$\tilde{f}_{j+\frac{1}{2}} = \tilde{f}_{j+\frac{1}{2}}^+ + \tilde{f}_{j+\frac{1}{2}}^-. \tag{2.16}$$

Third order TVD Runge–Kutta method, which is proposed by Shu and Osher [27], is used for time discretization in this paper. We write Eq. (2.2) as an ordinary differential equation (ODE) system

$$u_t = L(u), \tag{2.17}$$

where  $L(u)$  is a discretization of spatial operator. The general form of third order TVD Runge–Kutta method is as follow:

$$\begin{aligned} u^{(1)} &= u^n + \Delta t L(u^n) \\ u^{(2)} &= \frac{3}{4}u^n + \frac{1}{4}u^{(1)} + \frac{1}{4}\Delta t L(u^{(1)}) \\ u^{n+1} &= \frac{1}{3}u^n + \frac{2}{3}u^{(2)} + \frac{2}{3}\Delta t L(u^{(2)}). \end{aligned} \tag{2.18}$$

### 2.2 Finite Difference HWENO Schemes and CHWENO Schemes for Scalar Equation

In this section, we firstly introduce the finite difference HWENO scheme of Liu and Qiu [16], and then use it as our basis to structure finite difference CHWENO schemes for hyperbolic conservation laws (1.1). The ideas of HWENO schemes and CHWENO schemes are similar to WENO schemes, thus here we mainly focus on their different reconstruction processes.

In finite difference HWENO schemes [16], defining  $v = u_x$ , Liu and Qiu firstly get the derivative of Eq. (2.1) as follow:

$$\begin{cases} u_t + f(u)_x = 0, & u(x, 0) = u_0(x), \\ v_t + h(u, v)_x = 0, & v(x, 0) = v_0(x), \end{cases} \tag{2.19}$$

where  $h(u, v) = f(u)_x = f'(u)u_x = f'(u)v$ . To solve (2.19), they use a semi-discrete conservative approximation of the spatial derivatives:

$$\begin{cases} \frac{du_j(t)}{dt} = -\frac{\bar{f}_{j+\frac{1}{2}} - \bar{f}_{j-\frac{1}{2}}}{\Delta x}, \\ \frac{dv_j(t)}{dt} = -\frac{\bar{h}_{j+\frac{1}{2}} - \bar{h}_{j-\frac{1}{2}}}{\Delta x}, \end{cases} \tag{2.20}$$

where numerical fluxes  $\bar{f}_{j+1/2}$  and  $\bar{h}_{j+1/2}$  can be obtained by the following equations:

$$\begin{aligned} \bar{f}_{j+1/2} &= \bar{f}(u_{j-r}, \dots, u_{j+s}, v_{j-r}, \dots, v_{j+s}), \\ \bar{h}_{j+1/2} &= \bar{h}(u_{j-r}, \dots, u_{j+s}, v_{j-r}, \dots, v_{j+s}). \end{aligned} \tag{2.21}$$

It can be seen that two different numerical fluxes  $\bar{f}_{j+1/2}$  and  $\bar{h}_{j+1/2}$  need to be solved by the function values  $u_i$  and their derivatives  $v_i$  in finite difference HWENO scheme by Liu [16]. Similar to WENO schemes, we take fifth-order HWENO scheme as an example. Due to the lead-in of derivative values, we could get a fifth-order numerical flux  $\bar{f}_{j+1/2}$  in three points based on Hermite polynomials. This method will be introduced in detail later. Then we can see that HWENO schemes are more compact than WENO schemes because HWENO schemes use less points to obtain the numerical flux with same order accuracy. But the drawback is that HWENO schemes need to solve one more numerical flux  $\bar{h}_{j+1/2}$ , and the method is introduced in [16].

Therefore, in order to simplify the reconstruction procedure and maintain the compactness of HWENO schemes, this paper proposed finite difference CHWENO schemes, in which only one numerical flux  $\bar{f}_{j+1/2}$  need to be constructed. In CHWENO schemes, the spatial derivatives are directly approximated by the same semi-discrete conservative form with WENO schemes:

$$\frac{du_j(t)}{dt} = -\frac{\bar{f}_{j+\frac{1}{2}} - \bar{f}_{j-\frac{1}{2}}}{\Delta x}. \tag{2.22}$$

Similar to HWENO schemes, numerical flux  $\bar{f}_{j+1/2}$  is structured by  $u_i$  and their derivatives  $u'_i$  as follow:

$$\bar{f}_{j+1/2} = \bar{f}\left(u_{j-r}, \dots, u_{j+s}, u'_{j-r}, \dots, u'_{j+s}\right). \tag{2.23}$$

But difference is that in CHWENO schemes, the derivatives  $u'_i$  are directly obtained by compact difference schemes [15].

Now we will specifically introduce the reconstruction procedure of numerical flux in CHWENO schemes.

Step 1. We firstly present the compact difference methods that are used to obtain the derivative values of function.

- 1.1 Following the idea of [16], if the finite difference HWENO schemes achieve  $r$ th-order accuracy, the derivative equations should attain  $(r - 1)$ th-order accuracy. In other words, as for a class of fifth-order CHWENO schemes, the compact difference scheme to solve the derivative values should be at least a fourth-order scheme. Thus, for the every  $u_j$ , we choose the fourth-order central compact difference scheme [15]:

$$\frac{1}{6}u'_{j+1} + \frac{4}{6}u'_j + \frac{1}{6}u'_{j-1} = \frac{u_{j+1} - u_{j-1}}{2\Delta x} \tag{2.24}$$

as the method to solve the first derivative values of function.

- 1.2 To ensure the closure of compact difference scheme, some special methods need to be implemented near the boundary. We first consider a third-order upwind compact difference scheme [24]:

$$\begin{aligned} \frac{2}{3}u'_j + \frac{1}{3}u'_{j-1} &= \frac{1}{6}\frac{u_{j+1} - u_j}{\Delta x} + \frac{5}{6}\frac{u_j - u_{j-1}}{\Delta x}, \\ \frac{1}{3}u'_{j+1} + \frac{2}{3}u'_j &= \frac{5}{6}\frac{u_{j+1} - u_j}{\Delta x} + \frac{1}{6}\frac{u_j - u_{j-1}}{\Delta x}, \end{aligned} \tag{2.25}$$

which could reduce the accuracy of the derivative values near the boundary. The complete algorithm in the whole grid ( $j = 1, \dots, n$ ) is as below:

$$\begin{cases} \frac{2}{3}u'_2 + \frac{1}{3}u'_1 = \frac{1}{6}\frac{u_3 - u_2}{\Delta x} + \frac{5}{6}\frac{u_2 - u_1}{\Delta x}, \\ \frac{1}{6}u'_{j+1} + \frac{4}{6}u'_j + \frac{1}{6}u'_{j-1} = \frac{u_{j+1} - u_{j-1}}{2\Delta x}, \quad (j = 2, \dots, n - 1), \\ \frac{1}{3}u'_n + \frac{2}{3}u'_{n-1} = \frac{5}{6}\frac{u_n - u_{n-1}}{\Delta x} + \frac{1}{6}\frac{u_{n-1} - u_{n-2}}{\Delta x}. \end{cases} \tag{2.26}$$

In this way we get a set of tridiagonal systems, which is composed of fourth-order central compact difference scheme in the interior points and third-order upwind compact difference scheme at the boundary. For simplicity, we term the CHWENO schemes with this method as CHWENO4 schemes.

- 1.3 Another method to get the derivative values at the boundary is increasing the function terms in the right side of equation, which could avoid order reduction. We consider the eccentric compact difference:

$$\alpha u'_{j-1} + \beta u'_j = \frac{1}{\Delta x} (a u_{j-1} + b u_j + c u_{j+1} + d u_{j+2}). \tag{2.27}$$

We let  $\beta = 1$  without loss generality. Then we get Taylor expansion for the right terms and get the linear equations as below:

$$\begin{cases} a + b + c + d = 0, \\ -a + c + 2d = \alpha + 1, \\ \frac{1}{2}a + \frac{1}{2}c + 2d = -\alpha, \\ -\frac{1}{6}a + \frac{1}{6}c + \frac{4}{3}d = \frac{1}{2}\alpha, \\ \frac{1}{24}a + \frac{1}{24}c + \frac{2}{3}d = -\frac{1}{6}\alpha. \end{cases} \tag{2.28}$$

The coefficients could be gotten by solving the equations, and then we could derive a fourth-order bias compact difference scheme

$$\frac{1}{3}u'_{j-1} + u'_j = \frac{1}{18\Delta x} (-17u_{j-1} + 9u_j + 9u_{j+1} - u_{j+2}), \tag{2.29}$$

which could be used at the left boundary. Similarly,

$$u'_j + \frac{1}{3}u'_{j+1} = \frac{1}{18\Delta x} (u_{j-2} - 9u_{j-1} - 9u_j + 17u_{j+1}) \tag{2.30}$$

is used at the right boundary. Therefore, we get the whole algorithm as below:

$$\begin{cases} \frac{1}{3}u'_1 + u'_2 = \frac{1}{18\Delta x} (-17u_1 + 9u_2 + 9u_3 - u_4) \\ \frac{1}{6}u'_{j-1} + \frac{4}{6}u'_j + \frac{1}{6}u'_{j+1} = \frac{u_{j+1} - u_{j-1}}{2\Delta x}, \quad (j = 2, \dots, m - 1) \\ u'_{m-1} + \frac{1}{3}u'_m = \frac{1}{18\Delta x} (u_{m-3} - 9u_{m-2} - 9u_{m-1} + 17u_m). \end{cases} \tag{2.31}$$

Then we can get the derivative values, which maintain uniformly fourth-order accuracy at all grid points. For simplicity, we term the CHWENO schemes with this method as CHWENO5 schemes.

In CHWENO schemes, we solve these tridiagonal systems (2.26), (2.31) by chasing method, which is more concise than HWENO schemes. In Sect. 4, we will test the accuracy, stability and other properties of both CHWENO4 and CHWENO5 schemes.

Step 2. Then we describe how to reconstruct the numerical flux  $\bar{f}_{j+1/2}^+$  by using both function values  $u_j$  and first derivative values  $u'_j$  gotten in Step 1.

2.1 Firstly, according to LF flux splitting (2.7), we can get the numerical fluxes of function values and derivative values as below:

$$\begin{cases} f_j^+ = \frac{1}{2} [f(u_j) + \alpha u_j] \\ f_j^{'+} = \frac{1}{2} [f'(u_j) + \alpha] u'_j \end{cases} \tag{2.32}$$

2.2 Unlike the Lagrange interpolation in WENO schemes, Hermite interpolation is used in the reconstruction of HWENO and CHWENO schemes. In this way, less stencil points are used in the HWENO schemes and CHWENO schemes. We use the points and derivative values to construct three third-order numerical fluxes and then use these fluxes to construct a more accurate numerical flux. For this purpose, we



choose three small stencils  $S_1 = \{I_{j-1}, I_j, I'_{j-1}\}$ ,  $S_2 = \{I_j, I_{j+1}, I'_{j+1}\}$ ,  $S_3 = \{I_{j-1}, I_j, I_{j+1}\}$ , which are used to structure a bigger stencil  $S = S_1 \cup S_2 \cup S_3 = \{I'_{j-1}, I_{j-1}, I_j, I_{j+1}, I'_{j+1}\}$ .

For the small stencil  $S_i$ , we use Hermite polynomials to formulate the function  $p_i(x)$  to get the function value at the half nodes  $x_{j+1/2}$ . Hence, we have

$$\begin{aligned} p_1(x_{j+1/2}) &= -\frac{7}{6}f_{j-1}^+ + \frac{13}{6}f_j^+ - \frac{2\Delta x}{3}f'_{j-1}, \\ p_2(x_{j+1/2}) &= \frac{1}{6}f_j^+ + \frac{5}{6}f_{j+1}^+ - \frac{\Delta x}{3}f'_{j+1}, \\ p_3(x_{j+1/2}) &= -\frac{1}{6}f_{j-1}^+ + \frac{5}{6}f_j^+ + \frac{1}{3}f'_{j+1}. \end{aligned} \tag{2.33}$$

For the bigger stencil  $S$ , we can also get the function  $q(x)$  through Hermite polynomials. Then we get a fifth-order numerical flux

$$\begin{aligned} q\left(x_{j+\frac{1}{2}}\right) &= -\frac{23}{120}f_{j-1}^+ + \frac{19}{30}f_j^+ + \frac{67}{120}f_{j+1}^+ \\ &\quad - \Delta x \left( \frac{3}{40}f'_{j-1} + \frac{7}{40}f'_{j+1} \right). \end{aligned} \tag{2.34}$$

2.3 On the smooth regions,  $q(x)$  has the highest order accuracy in the stencil  $S$ , so that an important step in CHWENO reconstruction is to solve the optimal weights that combine  $p_1(x)$ ,  $p_2(x)$  and  $p_3(x)$  into  $q(x)$  at  $x = x_{j+1/2}$ . The linear weights are denoted by  $C_i^+$  for stencil  $S_i$  satisfying

$$\begin{cases} q(x_{j+1/2}) = \sum_1^3 C_i^+ p(x_{j+1/2}), \\ \sum_1^3 C_i^+ = 1. \end{cases} \tag{2.35}$$

By Eq. (2.35) we can get

$$C_1^+ = \frac{9}{80}, \quad C_2^+ = \frac{42}{80}, \quad C_3^+ = \frac{29}{80}. \tag{2.36}$$

2.4 For the excellent property near the discontinuities, we also need to compute the smoothness measurement, indicated by  $IS_i^+$  for stencil  $S_i$ . In this paper, we adopt the method in [22] to calculate the smoothness measurement as follow:

$$IS_i^+ = \sum_{l=1}^2 \int_{x_{j-1/2}}^{x_{j+1/2}} (\Delta x)^{2l-1} \left( \frac{\partial^l p_i}{\partial x^l} \right)^2 dx \tag{2.37}$$

Through using Eq. (2.37), smoothness measurement expressions are

$$\begin{aligned} IS_1^+ &= \left| 2(f_j^+ - f_{j-1}^+) - \Delta x \cdot (f')_{j-1}^+ \right|^2 \\ &\quad + \frac{13}{3} \left| (f_j^+ - f_{j-1}^+) - \Delta x \cdot (f')_{j-1}^+ \right|^2, \\ IS_2^+ &= \left| 2(f_{j+1}^+ - f_j^+) - \Delta x \cdot (f')_{j+1}^+ \right|^2 \end{aligned}$$

$$\begin{aligned}
 & + \frac{13}{3} \left| (f_{j+1}^+ - f_j^+) - \Delta x \cdot (f')_{j+1}^+ \right|^2, \\
 IS_3^+ & = \frac{1}{4} \left| f_{j+1}^+ - f_{j-1}^+ \right|^2 + \frac{13}{12} \left| f_{j+1}^+ - 2f_j^+ + f_{j-1}^+ \right|^2.
 \end{aligned}
 \tag{2.38}$$

2.5 In the smooth regions, we can use the optimal weights to improve the accuracy of CHWENO schemes, and the information of all stencils is used. While in the regions near discontinuities, the weights need to be adjusted by increasing the weights of smoother stencils. The smoother stencil has smaller smoothness measurement and hence bigger weights. Thus it plays a more important role in the convex combination. We assume

$$\alpha_r^+ = \frac{C_r^+}{(\varepsilon + IS_r^+)^2} \quad (r = 1, 2, 3),
 \tag{2.39}$$

where  $\varepsilon$  is an extremely low positive number whose purpose is to avoid the denominator being zero. In this paper, we let  $\varepsilon = 10^{-6}$ , and it is proved by the tests in [12] that the result is not sensitive to the value of  $\varepsilon$ . Then weight function  $\omega_r$  is gained after normalization processing:

$$\omega_r^+ = \frac{\alpha_r^+}{\alpha_1^+ + \alpha_2^+ + \alpha_3^+} \quad (r = 1, 2, 3).
 \tag{2.40}$$

The CHWENO reconstruction approximation is computed by

$$\bar{f}_{j+\frac{1}{2}}^+ = \omega_1^+ p_1^+ + \omega_2^+ p_2^+ + \omega_3^+ p_3^+.
 \tag{2.41}$$

The reconstruction of  $\bar{f}_{j+1/2}^-$  is symmetric to that of  $\bar{f}_{j+1/2}^+$ , and we can get  $\bar{f}_{j+1/2}^-$  by similar method.

2.6 Finally, the numerical flux can be gained by

$$\bar{f}_{j+\frac{1}{2}} = \bar{f}_{j+\frac{1}{2}}^+ + \bar{f}_{j+\frac{1}{2}}^-.
 \tag{2.42}$$

### 2.3 CHWENO Schemes for Vector Equations

Then we briefly introduce the extension of the CHWENO schemes to solve one-dimensional equations. We consider the equations as follow:

$$\frac{\partial \mathbf{u}}{\partial t} + \frac{\partial \mathbf{f}}{\partial x} = 0,
 \tag{2.43}$$

where  $\mathbf{u} = (u^1 \ u^2 \ \dots \ u^m)^T$ ,  $\mathbf{f} = (f_1(\mathbf{u}) \ f_2(\mathbf{u}) \ \dots \ f_m(\mathbf{u}))^T$ .

According to the mathematical property of hyperbolic equation, the Jacobian matrix of numerical flux  $\mathbf{A} = \partial \mathbf{f} / \partial \mathbf{u}$  can be decomposed as  $\mathbf{A} = \mathbf{RDR}^{-1}$ . In this  $\mathbf{D}$  is the diagonal matrix constructed by the eigenvalue of matrix  $\mathbf{A}$ .  $\mathbf{R}$  is the invertible matrix constructed by the eigenvector of matrix  $\mathbf{A}$ .

We let

$$\mathbf{q} = \mathbf{R}^{-1} \mathbf{f} \triangleq (q^1 \ q^2 \ \dots \ q^m)^T,
 \tag{2.44}$$

and we can get  $\mathbf{f} = \mathbf{RR}^{-1} \mathbf{f} = \mathbf{Rq}$ .

Then the CHWENO schemes in Sect. 2.2 are applied to every component of vector  $\mathbf{q}$ . Thus, we can use CHWENO schemes to solve the vector equations. In Sect. 4, some numerical experiments like one-dimensional Euler equations are solved in this way.

### 3 Descriptions of CHWENO Schemes in Two Dimensional Case

In this section, we develop the scheme in Sect. 2 to solve the two dimensional nonlinear hyperbolic conservation laws. First we consider 2D scalar equations

$$\begin{cases} u_t + f(u)_x + g(u)_y = 0, & (x, y) \in \mathbb{R}^2, t \in (0, \infty) \\ u(x, y, 0) = u_0(x, y), & (x, y) \in \mathbb{R}^2, \end{cases} \tag{3.1}$$

where  $u(x, y, t)$  is a conserved quantity, and  $f(u(x, y, t))$  and  $g(u(x, y, t))$  describes its flux in  $x$  direction and  $y$  direction, respectively. We define  $x_j = j \Delta x, y_k = k \Delta y$ .

In the finite difference HWENO schemes by Liu [16], they define  $v = u_x, w = u_y$ , taking the derivative  $x$  and  $y$  of (3.1) separately, and then get the whole equations form as below:

$$\begin{cases} u_t + f(u)_x + g(u)_y = 0, \\ v_t + h(u, v)_x + r(u, v)_y = 0, \\ w_t + q(u, w)_x + s(u, w)_y = 0, \end{cases} \tag{3.2}$$

where

$$\begin{aligned} h(u, v) &= f'(u) v, & r(u, v) &= g'(u) v, \\ q(u, w) &= f'(u) w, & s(u, w) &= g'(u) w. \end{aligned}$$

Again they approximate (3.2) by the following form:

$$\begin{cases} \frac{du_{j,k}(t)}{dt} = -\frac{\bar{f}_{j+\frac{1}{2},k} - \bar{f}_{j-\frac{1}{2},k}}{\Delta x} - \frac{\bar{g}_{j,k+\frac{1}{2}} - \bar{g}_{j,k-\frac{1}{2}}}{\Delta y}, \\ \frac{dv_{j,k}(t)}{dt} = -\frac{\bar{h}_{j+\frac{1}{2},k} - \bar{h}_{j-\frac{1}{2},k}}{\Delta x} - \frac{\bar{r}_{j,k+\frac{1}{2}} - \bar{r}_{j,k-\frac{1}{2}}}{\Delta y}, \\ \frac{dw_{j,k}(t)}{dt} = -\frac{\bar{q}_{j+\frac{1}{2},k} - \bar{q}_{j-\frac{1}{2},k}}{\Delta x} - \frac{\bar{s}_{j,k+\frac{1}{2}} - \bar{s}_{j,k-\frac{1}{2}}}{\Delta y}, \end{cases} \tag{3.3}$$

where numerical fluxes  $\bar{f}_{i\pm 1/2,j}, \bar{g}_{i,j\pm 1/2}, \bar{h}_{i\pm 1/2,j}$  and  $\bar{s}_{i,j\pm 1/2}$ , were straightforward reconstructed by the one dimensional methods in a dimension-by-dimension fashion. However, because of the existence of derivative equations, the key point of extending HWENO schemes to two dimensional cases is to construe the fluxes of mixed derivative terms,  $\bar{q}_{i\pm 1/2,j}$  and  $\bar{r}_{i,j\pm 1/2}$ . In [16], a 3-point WENO reconstruction is implemented in the mixed derivative terms and reduces the accuracy of two dimensional HWENO schemes to fourth order.

In finite difference CHWENO schemes, the derivative values are obtained by more convenient methods, compact difference schemes. So we do not need to reconstruct the fluxes of mixed derivative terms or reduce the accuracy order of schemes. In other words, we can use CHWENO schemes in a dimension-by-dimension fashion, just like WENO schemes, to solve the numerical fluxes in both  $x$  and  $y$  direction. Therefore, we directly obtain the semi-discrete conservative form of (3.1) as follow:

$$\frac{du_{j,k}(t)}{dt} = -\frac{\bar{f}_{j+\frac{1}{2},k} - \bar{f}_{j-\frac{1}{2},k}}{\Delta x} - \frac{\bar{g}_{j,k+\frac{1}{2}} - \bar{g}_{j,k-\frac{1}{2}}}{\Delta y}, \tag{3.4}$$

where the numerical fluxes  $\bar{f}_{j\pm 1/2,k}, \bar{g}_{j,k\pm 1/2}$  can be straightforward reconstructed by the CHWENO schemes in Sect. 2.

Thus it can be seen that in the two dimensional cases, CHWENO schemes have two major advantages over HWENO schemes. One is the efficiency, which means that there are only two fluxes reconstructed in CHWENO schemes, while six numerical fluxes need to be reconstructed in HWENO schemes. The other merit is that CHWENO schemes maintain fifth-order accuracy, while HWENO schemes have to reduce the accuracy to fourth order. The two-dimensional vector equations are solved in the same way of one-dimensional equations. For simplicity, they will not be described in details. In Sect. 4, we will test the accuracy and other properties of two dimensional CHWENO5 schemes.

## 4 Numerical Results

In this section, a number of numerical experiments are implemented to test the performance of finite difference CHWENO schemes. In order to facilitate the contrast analysis, HWENO schemes are also tested under the same conditions in every numerical experiment. For all the numerical tests in this paper, the third-order Runge–Kutta method (2.18) is used as time-stepping scheme, and CFL is set to be 0.8 in every test, except for the accuracy tests, where the time step is reduced to guarantee that spatial error dominates. Besides, we find that CFL number has little effect on the computing results of CHWENO5 schemes.

### 4.1 Scalar Conservation Laws in One Dimension

*Example 4.1 The linear advection problem* We consider the linear advection equation:

$$\begin{cases} u_t + u_x = 0, & -1 \leq x < 1, t > 0, \\ u(x, 0) = u_0(x). \end{cases} \quad (4.1)$$

The exact solution of this equation is  $u(x, t) = u_0(x - t)$ .

We would like to test the accuracy of CHWENO schemes by this problem. For this reason, we use CHWENO schemes to solve this problem with the initial condition:

$$u(x, 0) = \sin(\pi x). \quad (4.2)$$

The boundary condition we used is periodic boundary condition. We compute the solution up to  $t = 2$  with 10, 20, 40, 80, 160, 320 grid points, respectively. The  $L_1$ ,  $L_\infty$  errors and numerical orders by CHWENO4, CHWENO5 and HWENO5 schemes are shown in Table 1.

From the Table 1, we can see that both HWENO5 and CHWENO5 schemes achieve their designed order of accuracy. Under the same grid numbers, the numerical errors by CHWENO5 schemes are similar to that of HWENO5 schemes. However, CHWENO4 is a fourth-order scheme. Thus, the computing accuracy of whole schemes can be affected by the computing methods at the boundary. In order to get a fifth-order CHWENO scheme, fourth-order derivative values should be obtained in both interior points and boundaries.

*Example 4.2 Convex  $f(u)$  with smooth initial data* In this example, we test CHWENO schemes on nonlinear Burgers' equation

$$\begin{cases} u_t + (u^2/2)_x = 0, \\ u(x, 0) = 0.5 + \sin(\pi x), \end{cases} \quad (4.3)$$

with periodic boundary conditions.

**Table 1** Linear equation

N	$L_1$ error	Order	$L_\infty$ error	Order
<i>HWENO5</i>				
10	1.52E-02		2.50E-02	
20	5.70E-04	4.735000	1.14E-03	4.459242
40	1.70E-05	5.070433	3.35E-05	5.083640
80	5.28E-07	5.004165	1.08E-06	4.956649
160	1.65E-08	4.997505	3.25E-08	5.052796
320	5.22E-10	4.986068	9.71E-10	5.066969
<i>CHWENO4</i>				
10	1.81E-02		2.87E-02	
20	1.31E-03	3.787250	2.29E-03	3.644104
40	7.52E-05	4.120346	1.28E-04	4.164600
80	4.37E-06	4.103622	7.17E-06	4.156436
160	2.60E-07	4.071024	4.18E-07	4.099403
320	1.53E-08	4.083894	2.43E-08	4.105372
<i>CHWENO5</i>				
10	2.12E-02		3.53E-02	
20	6.94E-04	4.933278	1.37E-03	4.684848
40	1.98E-05	5.127338	4.02E-05	5.093878
80	5.90E-07	5.072605	1.17E-06	5.107150
160	1.79E-08	5.045820	3.40E-08	5.102311
320	5.52E-10	5.014348	9.87E-10	5.104031

$L_1, L_\infty$  errors and numerical orders of accuracy are measured at each point. Using N equally divided cells

The solution is still smooth when  $T = 0.5/\pi$ , and the numerical errors and accuracy orders by CHWENO4, CHWENO5 and HWENO schemes are shown in Table 2. We can see that the CHWENO4 and CHWENO5 schemes achieve their designed accuracy orders. The errors and accuracy orders of CHWENO5 schemes are similar to HWENO5 schemes under the same grids. When  $T = 1.5/\pi$ , the discontinuity occurs in the solution. So we show the numerical results of CHWENO schemes and HWENO schemes with  $N = 80$  in Fig. 1. We can see that in this case CHWENO schemes and HWENO schemes have similar resolution.

### 4.2 Euler System of Gas Dynamics in One Dimension

In this subsection, CHWENO schemes are used to solve the one dimensional system of the Euler equations for gas dynamic in conservation form:

$$\frac{\partial \mathbf{u}}{\partial t} + \frac{\partial \mathbf{f}}{\partial x} = 0, \tag{4.4}$$

where

$$\mathbf{u} = \begin{pmatrix} \rho \\ \rho u \\ E \end{pmatrix}, \quad \mathbf{f} = \begin{pmatrix} \rho u \\ \rho u^2 + p \\ (E + p)u \end{pmatrix}. \tag{4.5}$$

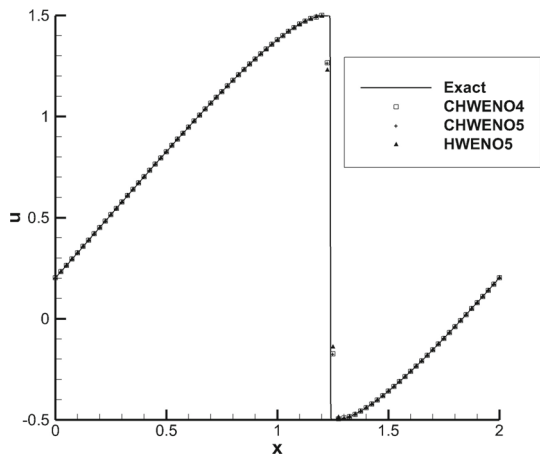
Here  $\rho$  is the density,  $p$  is the pressure,  $u$  is the velocity in  $x$  direction and  $E$  is the total energy. And the ideal gas equation is  $E = \frac{1}{\gamma-1}p + \frac{1}{2}\rho u^2$  with  $\gamma = 1.4$ . For simplicity, the

**Table 2** Burgers' equation

N	$L_1$ error	Order	$L_\infty$ error	Order
<i>HWENO5</i>				
10	1.47E-02		6.67E-02	
20	1.20E-03	3.612764	7.90E-03	3.078595
40	5.20E-05	4.532623	4.77E-04	4.048760
80	1.68E-06	4.955303	1.66E-05	4.843418
160	6.10E-08	4.781522	6.49E-07	4.678246
320	1.73E-09	5.139145	3.17E-08	4.357938
<i>CHWENO4</i>				
10	1.79E-02		8.43E-02	
20	2.38E-03	2.911245	1.35E-02	2.646531
40	1.71E-04	3.796341	1.60E-03	3.072645
80	7.89E-06	4.439976	7.47E-05	4.419762
160	4.81E-07	4.034124	5.12E-06	3.868791
320	2.76E-08	4.124956	4.72E-07	3.439106
<i>CHWENO5</i>				
10	1.59E-02		7.51E-02	
20	1.21E-03	3.715947	7.89E-03	3.249578
40	4.64E-05	4.704738	4.64E-04	4.088143
80	1.47E-06	4.980236	1.41E-05	5.040851
160	5.43E-08	4.758720	6.41E-07	4.458019
320	1.59E-09	5.093853	3.20E-08	4.326684

$L_1, L_\infty$  errors and numerical orders of accuracy are measured at each point. Using N equally divided cells

**Fig. 1** Numerical solution of the Burgers' equation as computed by the CHWENO4, CHWENO5 and HWENO5 with  $N = 80$  at  $T = 1.5/\pi$



Jacobian matrix, eigenvalue and eigenvectors that are used to solve this problem will not be shown in this paper.

*Example 4.3 Accuracy tests* Firstly, we would like to verify the accuracy order of CHWENO schemes when they are applied to solve the nonlinear system of Euler equations (4.4). We define the computing domain as  $[-1, 1]$  and the initial condition as  $\rho(x, 0) = 1 + 0.2 \sin(\pi x)$ ,  $p(x, 0) = 1$ ,  $u(x, 0) = 1$ . Periodic boundary conditions are used for

**Table 3** Euler equations

N	$L_1$ error	Order	$L_\infty$ error	Order
<i>HWENO5</i>				
10	5.42E-03		8.54E-03	
20	2.58E-04	4.392204	4.35E-04	4.295255
40	7.92E-06	5.028191	1.53E-05	4.829948
80	2.45E-07	5.011577	4.76E-07	5.005527
160	7.85E-09	4.966784	2.17E-08	4.457474
<i>CHWENO4</i>				
10	6.80E-03		9.75E-03	
20	4.02E-04	4.077986	6.45E-04	3.917224
40	1.87E-05	4.430208	3.70E-05	4.125907
80	9.47E-07	4.300453	1.55E-06	4.571525
160	5.30E-08	4.160940	8.44E-08	4.203335
<i>CHWENO5</i>				
10	6.52E-03		9.33E-03	
20	2.68E-04	4.605302	4.56E-04	4.356060
40	8.03E-06	5.059929	1.56E-05	4.871055
80	2.54E-07	4.983420	4.93E-07	4.979735
160	9.67E-09	4.714793	1.96E-08	4.655806

$L_1, L_\infty$  errors and numerical orders of accuracy are measured at each point. Using N equally divided cells

**Table 4** CPU time in seconds for HWENO and CHWENO schemes for Euler equations

N	CHWENO4	CHWENO5	HWENO5
100	0.68	0.65	0.83
400	10.74	10.25	11.36
1600	163.26	161.10	178.63

both the function values and derivative values. The exact solution of this problem is  $\rho(x, t) = 1 + 0.2 \sin(\pi(x - t)), p(x, t) = 1, u(x, t) = 1$ .

We also get the results at  $t = 2$  on uniform meshes having 10, 20, 40, 80, 160 points for HWENO and CHWENO schemes. In Table 3, we contrast the numerical errors of the density  $\rho$  by CHWENO schemes with HWENO schemes. One can obviously find that CHWENO5 and HWENO5 achieve fifth order of accuracy when they are applied to solve nonlinear Euler system, while CHWENO4 is still a fourth-order scheme. Then we display the CPU time of CHWENO4, CHWENO5 and HWENO schemes in Table 4. We observe that CHWENO4 and CHWENO5 schemes are a bit faster than HWENO5 scheme, which could save about 10% of CPU time.

Then we test the characteristics of CHWENO schemes with the problems involving very strong discontinuities.

*Example 4.4 Riemann Initial value Problems: Lax and sod’s problem* In this example, we test CHWENO schemes by two well-known problems of the Riemann initial value problems:

$$\mathbf{u}(x, 0) = \begin{cases} \mathbf{u}_L, & x < 0 \\ \mathbf{u}_R, & x > 0 \end{cases} \tag{4.6}$$

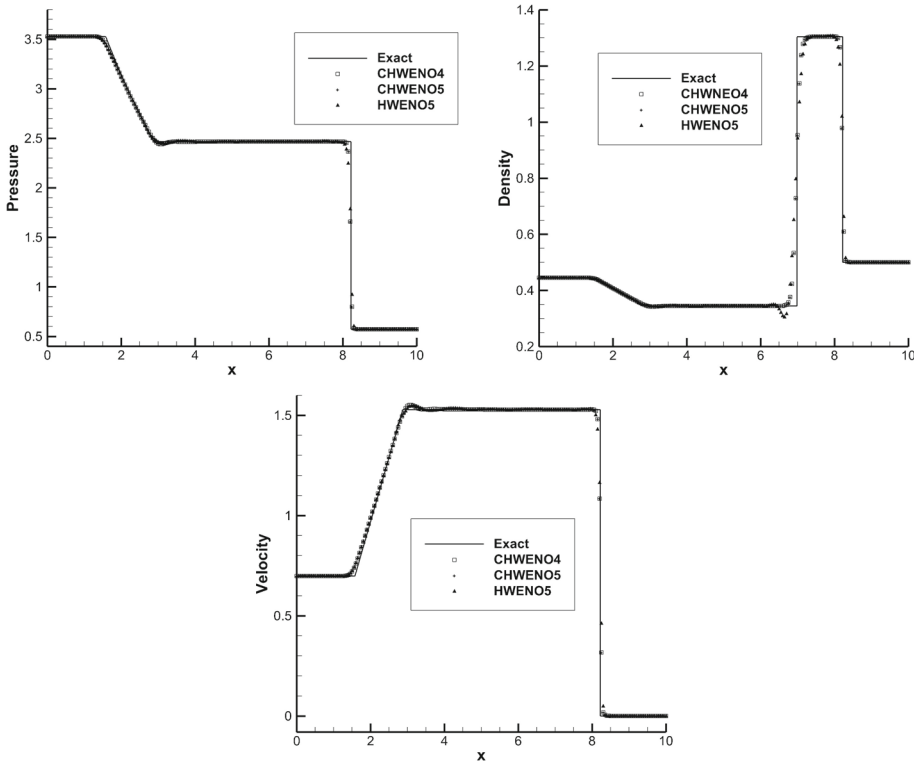


**Fig. 2** Numerical solution of the Lax problem with the Riemann initial condition as computed by the CHWENO4, CHWENO5 and HWENO5 with  $N = 200$

One of the Riemann initial problems is Lax problems, whose initial conditions in the left and the right stages of the shock are:

$$\begin{cases} (\rho_L, u_L, p_L) = (0.445, 0.698, 3.528), & x < 0, \\ (\rho_R, u_R, p_R) = (0.5, 0, 0.571), & x > 0. \end{cases} \tag{4.7}$$

The other of the Riemann initial problems is Sod’s problems, whose initial conditions in the left and the right stages of the shock are:

$$\begin{cases} (\rho_L, u_L, p_L) = (1, 0, 1), & x < 0, \\ (\rho_R, u_R, p_R) = (0.125, 0, 0.1), & x > 0. \end{cases} \tag{4.8}$$

We define the final time as  $t = 1.3$  (for Lax problem) and  $t = 2$  (for Sod’s problem) for both problems separately. The computational domain is  $[0, 10]$ , and the dividing line is  $x = 5$ . The constant boundary conditions are used for both function values and derivative values. The numerical results are presented in Figs. 2 and 3, where symbols denote the numerical results and solid lines denote the exact solution. From the figures we can see that all the schemes maintain good characteristics in all flow fields. There is no oscillation near the discontinuities and we can get a sharp transition. Besides, we can see that CHWENO schemes improve the resolution of shock waves because of the compactness of CHWENO schemes.



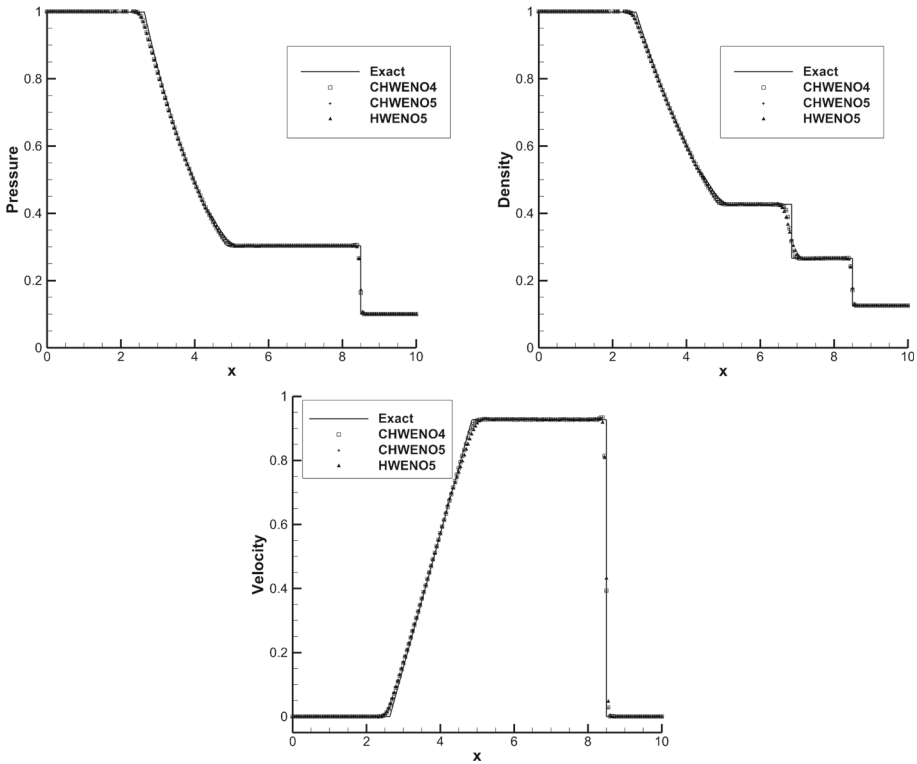


**Fig. 3** Numerical solution of the Sod’s problem with the Riemann initial condition as computed by the CHWENO4, CHWENO5 and HWENO5 with  $N = 200$

*Example 4.5 The shock density wave interaction problem* In this example, we consider the problem that involves both shocks and complex smooth regions. We need to solve the equation with a moving shock interacting with the sine waves in density, which is defined by the following initial conditions:

$$(\rho, u, p) = \begin{cases} (3.857143, 2.62936, 10.333333), & x < 1.0, \\ (1.0 + 0.2 \sin(5x), 0, 1.0), & x > 1.0, \end{cases} \tag{4.9}$$

where the computational domain is  $[0, 10]$ . We take periodic boundary for this problem, and the final time is  $t = 1.8$ . The results of CHWENO and HWENO schemes are compared under the same grid number  $N = 300$ . The exact solution of this problem is a converged solution computed by WENO5 with 2000 grid points.

Like other problems with shock and disconnect, what we really care are the resolution and sharp transition of the solution. From Fig. 4, we can see that the results of CHWENO schemes are more consistent with the exact solution than that of HWENO schemes, particularly at the waves near the shock. Thus through this example, we can verify the stability and accuracy of CHWENO schemes at the presence of shock and entropy waves. And the improvement of resolution in CHWENO schemes is apparent.

Then we also display the CPU times of CHWENO schemes and HWENO schemes on solving Lax, Sod’s and Shu-Osher problem in Table 5. We can see that in one dimensional cases, CHWENO schemes can improve the computational efficiency in some extent because

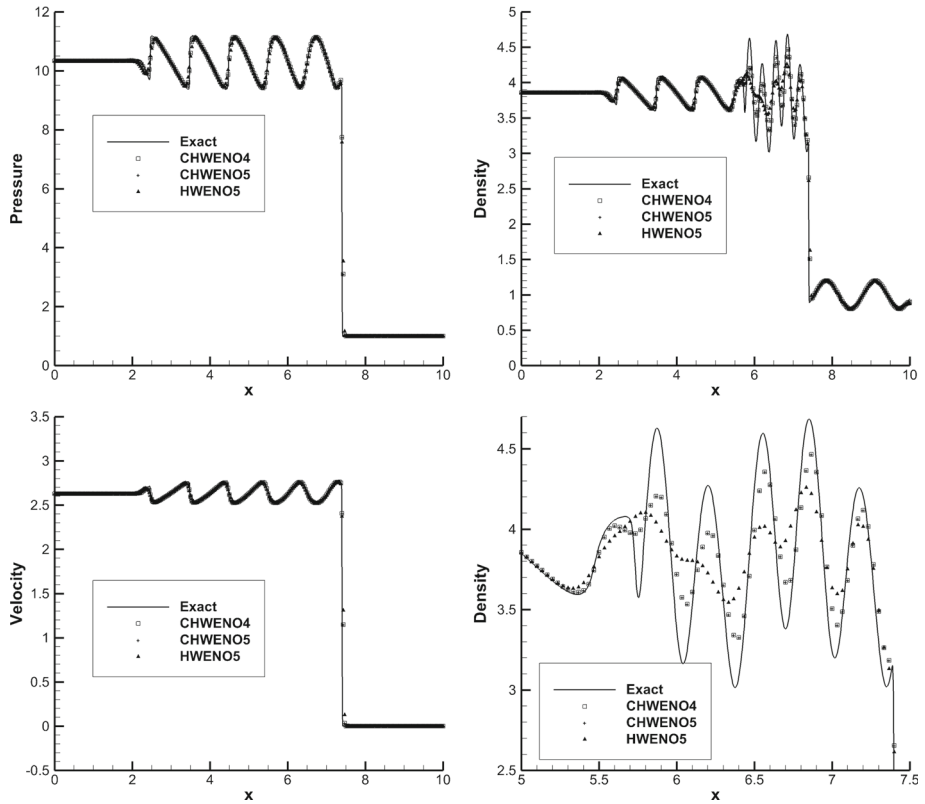


**Fig. 4** Numerical solution of the Shu and Osher problem with the Riemann initial condition as computed by the CHWENO4, CHWENO5 and HWENO5 with  $N = 300$

**Table 5** CPU time in seconds for HWENO and CHWENO schemes

	N	CHWENO4	CHWENO5	HWENO5
Lax problem	200	0.56	0.56	0.64
	800	8.68	8.69	9.28
Sod’s problem	200	0.41	0.42	0.47
	800	6.29	6.28	7.09
Shu and Osher problem	200	0.79	0.76	0.86
	800	12.12	12.20	13.12

we need to solve only one flux in CHWENO schemes but two fluxes in HWENO schemes. However, the efficiency of CHWENO schemes is not obvious because we also need to use compact difference schemes to obtain the derivative values. The efficiency of CHWENO schemes is more apparent in two dimensional cases, and we will show it in the next test.

### 4.3 Euler System of Gas Dynamics in two Dimensions

In this subsection, we test the CHWENO schemes in two dimensional cases. Firstly, the accuracy of CHWENO schemes is verified. Then, some numerical problems with complex

solution and discontinuities are used to test the characteristics of CHWENO schemes when there are strong discontinuities in the calculation. The conservation form of two dimensional Euler equations is as follow:

$$\frac{\partial \mathbf{q}}{\partial t} + \frac{\partial \mathbf{f}}{\partial x} + \frac{\partial \mathbf{g}}{\partial y} = 0, \tag{4.10}$$

where

$$\mathbf{q} = \begin{pmatrix} \rho \\ \rho u \\ \rho v \\ E \end{pmatrix}, \mathbf{f} = \begin{pmatrix} \rho u \\ \rho u^2 + p \\ \rho uv \\ (E + p)u \end{pmatrix}, \mathbf{g} = \begin{pmatrix} \rho v \\ \rho uv \\ \rho v^2 + p \\ (E + p)v \end{pmatrix}. \tag{4.11}$$

Here  $\rho$  is the density,  $p$  is the pressure,  $u$  is the velocity in  $x$  direction,  $v$  is the velocity in  $y$  direction and  $E$  is the total energy. And the ideal gas equation is  $E = \frac{1}{\gamma-1} p + \frac{1}{2} \rho (u^2 + v^2)$  with  $\gamma = 1.4$ . For simplicity, the Jacobian matrix, eigenvalue and eigenvectors that are used to solve this problem will not be shown in this paper. In every numerical test, we will only show the results by CHWENO5 scheme because the solution of CHWENO4 scheme is the same as CHWENO5 scheme.

*Example 4.6 Accuracy tests* Firstly, we would like to verify the accuracy order of CHWENO schemes when they are applied to solve the two dimensional nonlinear system of Euler equations (4.10). We define the computing domain as  $[0, 2] \times [0, 2]$  and the initial condition as  $\rho(x, y, 0) = 1 + 0.2 \sin(\pi(x + y))$ ,  $p(x, y, 0) = 1$ ,  $u(x, y, 0) = 0.7$ ,  $v(x, y, 0) = 0.3$ . Periodic boundary conditions are used for both the function values and derivative values. The exact solution of this problem is  $\rho(x, y, 0) = 1 + 0.2 \sin(\pi((x+y) - (u+v)t))$ ,  $p(x, y, t) = 1$ ,  $u(x, y, t) = 0.7$ ,  $v(x, y, t) = 0.3$ .

We get the results at  $t = 2$  on uniform meshes having  $10 \times 10, 20 \times 20, 40 \times 40, 80 \times 80, 160 \times 160$  points for HWENO and CHWENO schemes. In Table 6, we contrast the numerical errors of the density  $\rho$  by CHWENO schemes with those by HWENO schemes. One can obviously find that CHWENO5 achieves fifth order of accuracy when applied to solve two dimensional nonlinear Euler system, while CHWENO4 and HWENO schemes are still fourth-order schemes. Besides, the accuracy order of HWENO schemes can not achieve fourth order accuracy in the case of low mesh numbers, which can be also observed in [16]. Thus comparing with the HWENO schemes, in two dimensional cases, the extension of CHWENO schemes from one dimensional cases to two dimensional cases does not reduce the order of accuracy.

Then we display the CPU time of HWENO and CHWENO schemes for solving two dimensional Euler equations in Table 7. From it we can see the CHWENO schemes are about two times as fast as HWENO schemes for 2D Euler problem. CHWENO schemes greatly improve the efficiency in two dimensional cases because HWENO schemes need to solve more numerical fluxes, including two mixed derivative terms which do not appear in CHWENO schemes.

*Example 4.7 2D Riemann problem* In this example, we test the characteristics of two dimensional CHWENO schemes when solving problems with strong discontinuities, i.e. two dimensional Riemann problems. In this paper, we solve four two dimensional Riemann problems, whose initial conditions are as follow, respectively:

**Table 6** The two-dimensional Euler equations

$N \times M$	$L_1$ error	Order	$L_\infty$ error	Order
<i>HWENO</i>				
$10 \times 10$	2.01E-02		3.50E-02	
$20 \times 20$	4.57E-03	2.132785	1.17E-02	1.579210
$40 \times 40$	1.53E-03	1.583913	4.40E-03	1.410472
$80 \times 80$	8.06E-05	4.241868	2.55E-04	4.107023
$160 \times 160$	5.00E-06	4.012415	1.45E-05	4.142834
<i>CHWENO4</i>				
$10 \times 10$	1.04E-02		1.72E-02	
$20 \times 20$	5.69E-04	4.189843	1.12E-03	3.934719
$40 \times 40$	2.41E-05	4.561021	6.01E-05	4.222138
$80 \times 80$	1.15E-06	4.395931	3.30E-06	4.184895
$160 \times 160$	6.67E-08	4.102191	2.10E-07	3.978161
<i>CHWENO5</i>				
$10 \times 10$	9.38E-03		1.44E-02	
$20 \times 20$	4.15E-04	4.497391	7.03E-04	4.351672
$40 \times 40$	1.26E-05	5.046754	2.45E-05	4.840723
$80 \times 80$	4.00E-07	4.971863	8.02E-07	4.935174
$160 \times 160$	1.32E-08	4.924857	3.13E-08	4.681271

$L_1, L_\infty$  errors and numerical orders of accuracy are measured at each point. Using  $N \times M$  equally divided cells

**Table 7** CPU time in seconds for HWENO and CHWENO schemes for two dimensional Euler equations

$N \times M$	CHWENO4	CHWENO5	HWENO
$10 \times 10$	1.20	1.21	2.07
$40 \times 40$	57.86	59.05	98.69
$160 \times 160$	3573.29	3500.83	5902.25

$$a.(\rho, u, v, p)^T = \begin{cases} (0.5313, 0, 0, 0.4)^T, & x > 0.5, y > 0.5, \\ (1, 0.7276, 0, 1)^T, & x < 0.5, y > 0.5, \\ (0.8, 0, 0, 1)^T, & x < 0.5, y < 0.5, \\ (1, 0, 0.7276, 1)^T, & x > 0.5, y < 0.5, \end{cases} \quad (4.12)$$

$$b.(\rho, u, v, p)^T = \begin{cases} (1, 0.1, 0, 1)^T, & x > 0.5, y > 0.5, \\ (0.5313, 0.8276, 0, 0.4)^T, & x < 0.5, y > 0.5, \\ (0.8, 0.1, 0, 0.4)^T, & x < 0.5, y < 0.5, \\ (0.5313, 0.1, 0.7276, 0.4)^T, & x > 0.5, y < 0.5, \end{cases} \quad (4.13)$$

$$c.(\rho, u, v, p)^T = \begin{cases} (0.5313, 0.1, 0.1, 0.4)^T, & x > 0.5, y > 0.5, \\ (1.0222, -0.6179, 0.1, 1)^T, & x < 0.5, y > 0.5, \\ (0.8, 0.1, 0.1, 1)^T, & x < 0.5, y < 0.5, \\ (1, 0.1, 0.8276, 1)^T, & x > 0.5, y < 0.5, \end{cases} \quad (4.14)$$

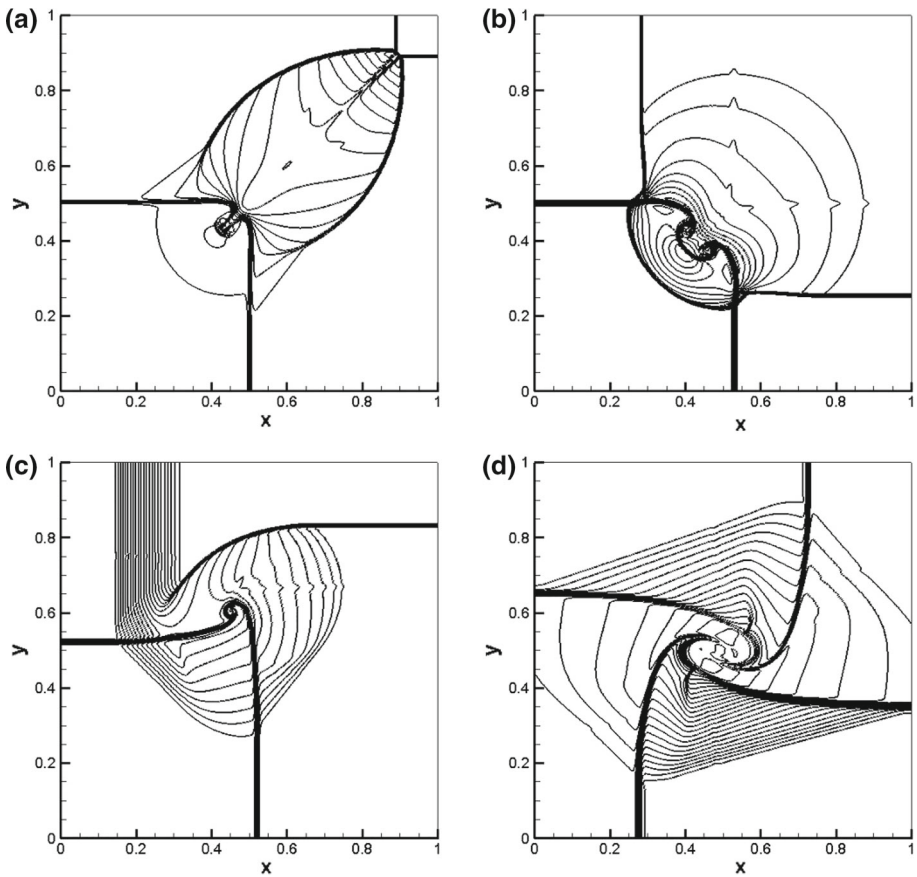


**Fig. 5** Numerical solution of the four Riemann problems computed by CHWENO5 with  $N \times M = 400 \times 400$ . 30 equally spaced density contours are plotted, respectively

$$d.(\rho, u, v, p)^T = \begin{cases} (1, 0.75, -0.5, 1)^T, & x > 0.5, y > 0.5, \\ (2, 0.75, 0.5, 1)^T, & x < 0.5, y > 0.5, \\ (1, -0.75, 0.5, 1)^T, & x < 0.5, y < 0.5, \\ (3, -0.75, -0.5, 1)^T, & x > 0.5, y < 0.5, \end{cases} \quad (4.15)$$

The computational domain is defined to be  $[0, 1] \times [0, 1]$ , with  $400 \times 400$  grid points. The final times are a.  $t = 0.25$ , b.  $t = 0.3$ , c.  $t = 0.2$ , d.  $t = 0.3$  for the four Riemann problems, respectively. The numerical results of CHWENO5 are shown in Fig. 5. It can be obviously seen that the results by CHWENO schemes are comparable with HWENO schemes in [16] and the structures of shock wave are well captured by CHWENO schemes. Thus we can prove that two dimensional CHWENO schemes keep good characteristics when applied to solve the problems with strong discontinuities.

*Example 4.8 A Mach 3 wind tunnel with a step* This model problem begins with uniform Mach 3 flow in a wind tunnel containing a step and has been introduced in detail in [29]. The setup of the problem is following: The wind tunnel is 1 length unit wide and 3 length units

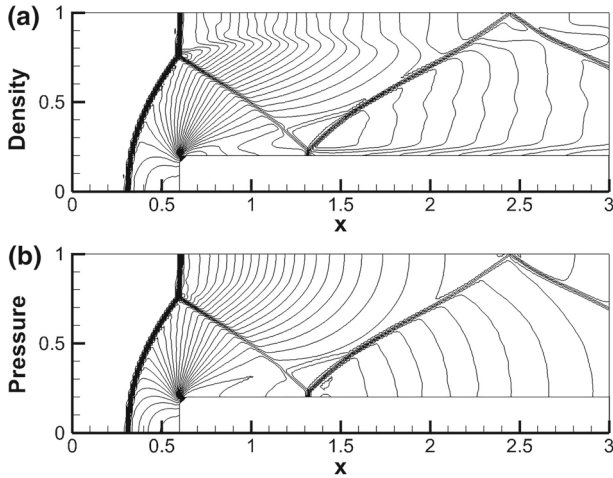


**Fig. 6** Forward step problem with  $N \times M = 240 \times 80$ . 30 equally spaced density and pressure contours from 0.32 to 6.3 and from 0.35 to 13, separately

long. The step is 0.2 length units high and is located 0.6 length units from the left-hand end of the tunnel. The problem is initialized by a right-going Mach 3 flow with the initial conditions,  $(p, \rho, u, v) = (1, 1.4, 3, 0)$ . Along the walls of the tunnel reflecting boundary conditions are applied. At the left is a flow-in boundary condition, and at the right all gradients are assumed to vanish. As for the singular point, we use the same methods in [29]. In Fig. 6, we show the density component obtained by CHWENO5 schemes at  $t = 4.0$  with 30 equally spaced density contours from 0.32 to 6.3, pressure contours from 0.35 to 13. We can see that the results of CHWENO5 scheme perform well and are similar to that of HWENO5 in [16].

*Example 4.9 Double Mach reflection* This problem is also originally from [29]. The flow can be set up experimentally by driving a shock down a tube which contains a wedge. The computational domain of this problem is  $[0, 4] \times [0, 1]$ . Our test problem involves a Mach 10 shock in air ( $\gamma = 1.4$ ) which initially makes a 60 angle with a reflecting wall at  $x = 1/6, y = 0$ . The undisturbed air ahead of the shock has a density of 1.4 and a pressure of 1. The region from  $x = 0$  to  $x = 1/6$  along the bottom boundary at  $y = 0$  is always assigned values for the initial post-shock flow, and the reflective boundary condition is used for the rest. The left-hand boundary is also assigned values for the initial post-shock flow, and at the right-hand boundary, at  $x = 4$ , all gradients are set to zero. At the top boundary, the flow values are set to describe the exact motion of a Mach 10 shock. The flow at time 0.2, computed by CHWENO5 scheme with two different uniform meshes  $480 \times 120$  and  $960 \times 240$ , is displayed in Fig. 7. Only the region between  $x = 0$  and  $x = 3$  is showed in the figure, although the grid continues to  $x = 4$ . Comparing with the results of HWENO5 in [16], we see that CHWENO schemes resolve the two Mach stems well.

*Example 4.10 Shock vortex interaction* In this example, we use the CHWENO schemes to test the problem of the interaction between a stationary shock and vortex. The computational domain is  $[0, 2] \times [0, 1]$ . A stationary Mach 1.1 shock is positioned at  $x = 0.5$  and normal to the  $x$ -axis. The initial left state is  $(p, \rho, u, v) = (1, 1, 1.1\sqrt{\gamma}, 0)$ . Its right state can be easily confirmed by Rankine–Hugoniot condition. A small vortex is superposed to the flow left to the shock and centers at  $(x_c, y_c) = (0.25, 0.5)$ . We define the vortex as a perturbation

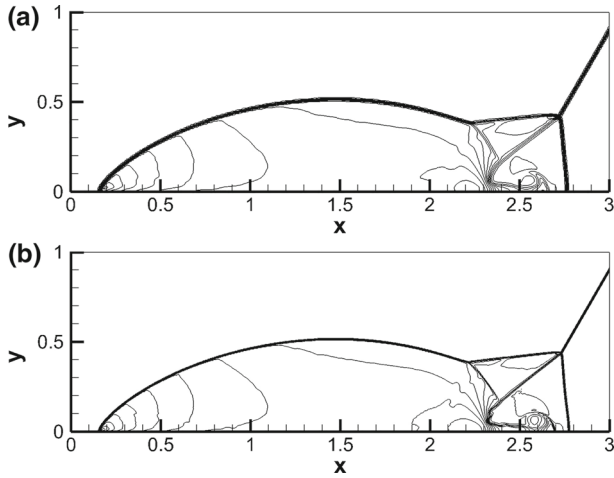


**Fig. 7** Density plot for double mach reflection with two different meshes. 30 equally spaced density contours from 0.9 to 22.6

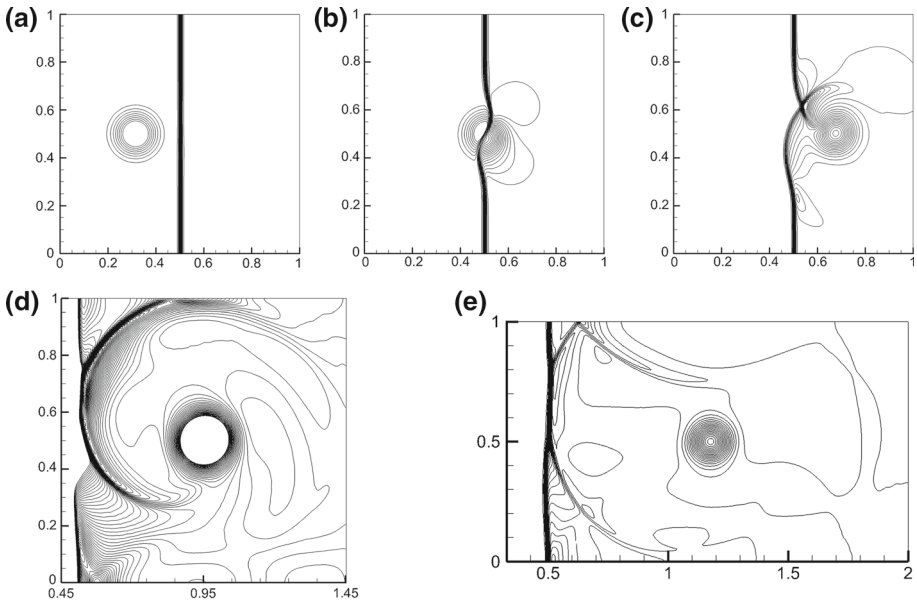


**Fig. 8** 2D shock vortex interaction. Pressure. 30 contours for **a–c** and **e**, **d** 90 contours. **a**  $t = 0.05$ , **b**  $t = 0.2$ , **c**  $t = 0.35$ , **d**  $t = 0.6$ , **e**  $t = 0.8$

to the velocity  $(u, v)$ , temperature  $T = (p/\rho)$  and entropy  $S = \ln(p/\rho^\gamma)$  of the mean flow and we can denote them by the following values:

$$\begin{cases} \tilde{u} = \varepsilon \tau e^{\alpha(1-\tau^2)} \sin \theta, \\ \tilde{v} = -\varepsilon \tau e^{\alpha(1-\tau^2)} \cos \theta, \\ \tilde{T} = -\frac{(\gamma-1)\varepsilon^2 e^{2\alpha(1-\tau^2)}}{4\alpha\gamma}, \\ \tilde{S} = 0, \end{cases} \tag{4.16}$$

where  $\tau = r/r_c$ ,  $r = \sqrt{(x - x_c)^2 + (y - c_c)^2}$ ,  $\varepsilon = 0.3$ ,  $r_c = 0.05$ ,  $\alpha = 0.204$ . Here  $\varepsilon$  indicates the strength of the vortex,  $\alpha$  controls the decay rates of the vortex, and  $r_c$  is the critical radius where the vortex has the maximum strength. We can see more details in [12, 26].

In our test, we use a uniform grid of  $251 \times 100$  in the computational domain. The reflective boundary conditions are used at the upper and lower boundaries. The in/out flow boundary conditions are applied at the left/right boundaries. The pressure contours obtained by CHWENO5 scheme at  $t = 0.05$ ,  $t = 0.2$ ,  $t = 0.35$ ,  $t = 0.6$ ,  $t = 0.8$  are shown in Fig. 8. We can see that CHWENO schemes can capture the vortex and shock well.

## 5 Concluding Remarks

Finite volume HWENO schemes were firstly introduced by Qiu and Shu [22, 23] in 2004, and finite difference HWENO schemes were proposed by Liu and Qiu [16, 17] in 2015. In this paper, we present a class of finite difference CHWENO schemes, which aim to simplify the reconstruction procedure of HWENO schemes. CHWENO reconstruction uses Hermite polynomials like HWENO schemes, but the derivative terms are straightforward obtained by compact difference schemes, which can considerably increase the computing speed, especially in two dimensional cases. Due to the different compact difference schemes which are used at boundary, we propose two methods, CHWENO4 and CHWENO5 schemes. Through numerical experiments, we find that CHWENO4 scheme is a fourth-order scheme and CHWENO5 is a fifth-order scheme, which means that treatment methods at boundary can affect the accuracy of whole scheme. Comparing with WENO schemes, CHWENO schemes maintain the compactness of HWENO schemes. For instance, only three points are needed in a fifth-order HWENO and CHWENO reconstruction, while five points are used in a fifth-order WENO reconstruction. And the good characteristics near discontinuities, like non-oscillatory property of WENO schemes, are well preserved in CHWENO schemes. Comparing with HWENO schemes, CHWENO schemes not only greatly improve the efficiency of calculation, but also avoid the order reduction of schemes in two dimensional cases.

### Compliance with Ethical Standards

**Conflict of interest** The authors declare that they have no conflict of interest.

## References

1. Adams, N.A., Shariff, K.: A high-resolution hybrid compact-ENO scheme for shock-turbulence interaction problems. *J. Comput. Phys.* **127**, 27–51 (1996)
2. Balsara, D.S., Shu, C.W.: Monotonicity preserving weighted essentially non-oscillatory schemes with increasingly high order of accuracy. *J. Comput. Phys.* **160**, 405–452 (2000)
3. Christofi, S.N.: The study of building blocks for essentially non-oscillatory (ENO) schemes. Ph.D. thesis, Brown University (1995)
4. De, A.K., Eswaran, V.: Analysis of a new high resolution upwind compact scheme. *J. Comput. Phys.* **218**, 398–416 (2006)
5. Dennis, S., Hudson, J.: Compact h4 finite-difference approximations to operators of Navier–Stokes type. *J. Comput. Phys.* **85**, 390–416 (1989)
6. Gaitonde, D., Shang, J.S.: Optimized compact-difference-based finite-volume schemes for linear wave phenomena. *J. Comput. Phys.* **138**, 617–643 (1997)
7. Harten, A.: High resolution schemes for hyperbolic conservation laws. *J. Comput. Phys.* **49**, 357–393 (1983)



8. Harten, A., Engquist, B., Osher, S., Chakravarthy, S.R.: Uniformly high order accurate essentially non-oscillatory schemes, III. *J. Comput. Phys.* **71**, 231–303 (1987)
9. Harten, A., Osher, S.: Uniformly high-order accurate nonoscillatory schemes. I. *SIAM J. Numer. Anal.* **24**, 279–309 (1987)
10. Iske, A., Sonar, T.: On the structure of function spaces in optimal recovery of point functionals for ENO-schemes by radial basis functions. *Numer. Math.* **74**, 177–201 (1996)
11. Jiang, G.S., Peng, D.: Weighted ENO schemes for Hamilton–Jacobi equations. *SIAM J. Sci. Comput.* **21**, 2126–2143 (1997)
12. Jiang, G.S., Shu, C.W.: Efficient implementation of weighted ENO schemes. *J. Comput. Phys.* **126**, 202–228 (1996)
13. Jocksch, A., Adams, N.A., Kleiser, L.: An asymptotically stable compact upwind-biased finite-difference scheme for hyperbolic systems. *J. Comput. Phys.* **208**, 435–454 (2005)
14. Lafon, F., Osher, S.: High order two dimensional non-oscillatory methods for solving Hamilton–Jacobi scalar equations. *J. Comput. Phys.* **123**, 235–253 (1996)
15. Lele, S.K.: Compact finite difference schemes with spectral-like resolution. *J. Comput. Phys.* **103**, 16–42 (1992)
16. Liu, H., Qiu, J.: Finite difference Hermite WENO schemes for hyperbolic conservation laws. *J. Sci. Comput.* **63**, 548–572 (2015)
17. Liu, H., Qiu, J.: Finite difference Hermite WENO schemes for conservation laws, II: an alternative approach. *J. Sci. Comput.* **66**, 598–624 (2016)
18. Liu, X., Zhang, S., Zhang, H., Shu, C.W.: A new class of central compact schemes with spectral-like resolution, I: linear schemes. *J. Comput. Phys.* **248**, 235–256 (2013)
19. Liu, X., Zhang, S., Zhang, H., Shu, C.W.: A new class of central compact schemes with spectral-like resolution, II: hybrid weighted nonlinear schemes. *J. Comput. Phys.* **284**, 133–154 (2015)
20. Liu, X.D., Osher, S., Chan, T.: Weighted essentially non-oscillatory schemes. *J. Comput. Phys.* **115**, 200–212 (1994)
21. Osher, S., Shu, C.W.: High-order essentially non-oscillatory schemes for Hamilton–Jacobi equations. *SIAM J. Numer. Anal.* **28**, 907–922 (1991)
22. Qiu, J., Shu, C.W.: Hermite WENO schemes and their application as limiters for Runge–Kutta discontinuous Galerkin method: one-dimensional case. *J. Comput. Phys.* **193**, 115–135 (2004)
23. Qiu, J., Shu, C.W.: Hermite WENO schemes and their application as limiters for Runge–Kutta discontinuous Galerkin method II: two-dimensional case. *Comput. Fluids* **34**, 642–663 (2005)
24. Ravichandran, K.: Higher order KFVS algorithms using compact upwind difference operators. *J. Comput. Phys.* **130**, 161–173 (1997)
25. Sengupta, T.K., Ganeriwal, G., De, S.: Analysis of central and upwind compact schemes. *J. Comput. Phys.* **192**, 677–694 (2003)
26. Shu, C.W.: *High Order Weighted Essentially Nonoscillatory Schemes for Convection Dominated Problems*. Society for Industrial and Applied Mathematics, Philadelphia (2009)
27. Shu, C.W., Osher, S.: Efficient implementation of essentially non-oscillatory shock-capturing schemes. *J. Comput. Phys.* **77**, 439–471 (1988)
28. Shu, C.W., Osher, S.: Efficient implementation of essentially non-oscillatory shock-capturing schemes, II. *J. Comput. Phys.* **83**, 32–78 (1989)
29. Woodward, P., Colella, P.: The numerical simulation of two-dimensional fluid flow with strong shocks. *J. Comput. Phys.* **54**, 115–173 (1984)
30. Zhu, J., Qiu, J.: A class of the fourth order finite volume Hermite weighted essentially non-oscillatory schemes. *Sci. China Ser. A Math.* **51**, 1549–1560 (2008)